



Small Scale Non-Invasive Imaging Using Magnetic Induction Tomography - Hardware Design

Muhammad Saiful Badri Mansor^{1,2}, Ruzairi Abdul Rahim^{2*}, Zulkarnay Zakaria³, Nor Muzakkir Nor Ayob⁴, Yusri Md. Yunus², Anita Ahmad²

¹Biomedical Engineer,
Gleneagles Hospital Medini, Johor, MALAYSIA

²Process Tomography Research Group, School of Electrical Engineering, Faculty Engineering,
Universiti Teknologi Malaysia, 81310 UTM, MALAYSIA

³School of Mechatronic,
Universiti Malaysia Perlis, 02600 Arau, Perlis, MALAYSIA

⁴Senior Hardware Engineer,
KAIFA Technology Malaysia Sdn. Bhd, Taman Perindustrian Cemerlang, Ulu Tiram, Johor, MALAYSIA

*Corresponding Author

DOI: <https://doi.org/10.30880/ijie.2020.12.08.003>

Received 26 December 2019; Accepted 21 January 2020; Available online 30 August 2020

Abstract: This study is conducted to preliminary image the conductivity profile through the development of small scale non-invasive Magnetic Induction Tomography (MIT) system. It is proved that the Magnetic Induction Tomography interested in mapping the passive electrical properties of materials; conductivity (σ), permittivity (ϵ) and permeability (μ) in both process and medical tomography. The system is realized by designing the functional ferrite-core coil sensors, electronic measurements circuits for excitation and receiving coil, data acquisition system for transferring the data to the PC and suitable image reconstruction algorithm for providing the conductivity distributions measurement. The important characteristic for excitation coil is the one that can maintain the stability the optimum sine wave frequency ranging from 400 kHz up to 10 MHz. The sine waves are fed to the excitation coil through the application of high current amplifier component respectively. In the experiments, the copper phantom represent as high conductivity material were placed into the region of interest. The initial 16 channels MIT consists of 8 excitation coils and 8 receiving coils stacked alternately. On the receiving circuit, the major problem is the weak secondary signal perturbation sensed by the receiving coil has been improved by placing the variable amplifier on each receiver. The enhancement of conductivity profile imaging has been made by using a common Linear Back Projection (LBP) algorithm. The measurement was done on single and dual arrangement of copper phantom aligns in random coordinate so that the sensitivity of the excitation and receiving coil sensor can be experimentally observed. The imaging's results show that the hardware's and algorithm used was capable to process the data captured at the receiver. The results obtained can be useful for further improvement and research towards magnetic induction tomography.

Keywords: Magnetic induction tomography, excitation coil, receiving coil

1. Introduction

Magnetic induction tomography can be exploited for many applications in either process tomography or medical imaging. The main reason for the widespread use of this type of tomography is its contactless measurement capability and the ability to image the spatial distribution of electrical conductivity and magnetic permeability within a region of interest [1]. Metal detection in the food industry and molten metal flow imaging are examples of MIT applications [2].

Most metals are high conductivity materials, which are suitable for magnetic detection sensors. Highly conductive flow imaging also uses MIT to guarantee smooth product flow in its process pipeline, since coil sensors are resistant to high temperatures. In non-destructive testing, magnetic flux leakage (MFL) is a common tool for metal crack defect detection, and uses the same principle as MIT. The principle of the technique is straightforward; a magnetic field is induced in the metal pipe wall, then if there is a leakage or defect, the sensor will sense a resultant defect in the field [3]. In addition, by using this technique, an inspection can be made in a cost-effective way as there is no need to stop the operational flow in the pipeline. This is especially important in the oil and gas fields.

In certain process plants, process tomography is required to improve the operation and design of the processes handling multi-component mixtures, by enabling boundaries between different components to be non-invasively imaged by sensors. Information on the flow regime, constituent phases and component concentrations in process vessels and pipelines are determined from the reconstructed images [4]. In medical tomography, MIT is important for various specific applications. Some examples are summarised as follows:

- Determining the hydration state of biological tissues, total body water measurement and body composition assessment [5, 6, 7,8]
- Tumour detection and monitoring [9, 10, 11]
- Brain oedema and cerebral stroke detection [12, 13]
- Measurement of blood coagulation rates [14, 15]
- Monitoring of cardiac and lung function [16]
- Determination of excess liver stores in liver [17]

In this research, magnetic induction tomography is used to non-invasively construct the image of the conductivity profile. The principal consideration before continuing to develop the circuit architecture is the design of coil sensors. The excitation coil must be able to pick-up sinusoidal wave signals from the function generator. This is important because the excitation coil is the source of the primary fields that will be used to produce a secondary field or induce eddy currents in the material under examination. In addition, the excitation coil must be designed to proper specifications, considering the number of turns, inner and outer diameter of the ferrite core, the diameter of the copper wire used and to ensure it can maintain the stability of the sine wave when the input frequency changes. In the literature, most researchers use an air-core coil as the transmitter for biomedical magnetic induction tomography, while others used a ferrite core coil. In this research, a ferrite-core coil was introduced since it can provide a stable primary field.

Noise is always the most significant disturbance in any instrumentation system. Noise is caused by the environment and adjacent electronic devices, and is usually impossible to eliminate entirely, but it can be minimised at the design stage. Various techniques can be adopted to reduce the effect of noise, such as using an electronic filter, or a physical filter such as an excitation coil screen with focusing capability. The secondary field originating from the eddy current effect in materials is very small in magnitude and easily influenced by the noise. The sine wave frequency supplied to the excitation coil can be increased in order to sense a weak secondary field. However, doing this also contributes to the noise and an unwanted measurement of the secondary field will be sensed by the receiving coil. Before the measurements are taken, calibrations are crucial, and may help to eliminate this unwanted sensed value. There are various image reconstruction algorithms that can be used with different techniques to suit the specific application of tomography implemented. The simplest and suitable reconstruction algorithm is selected to produce conductivity profile images to avoid any software difficulties.

2. Hardware

The hardware is the part of the system where measurements take place. All data captured by the front-end sensors and the respective measurement architectures are acquired by the software as they are required to perform the image reconstruction. This chapter details the prototype work carried out for design of the coil sensors and the sensor jig setup. The complete workbench was composed of the sensor measuring area and the electronic measurement circuits.

2.1 Excitation and Receiving Coil

Most of the previous research in MIT focused on two main designs of the coil sensor, the air core and the ferromagnetic core [18]. The low sensitivity of an air coil sensor can be partially overcome by incorporation of a

ferromagnetic core, which acts as a flux concentrator inside the coil. The coil with a ferrite core provides a more stable and concentrated field, while coil without a ferrite core produces a less concentrated field. In this experiment, the excitation coil receives an alternating sine wave at 500 kHz to generate a magnetic field. Figure 1 shows an excitation coil with a square-type electromagnetic field screen. The excitation coil manufactured by EPCOS (82131) features a single-layer winding of enamel copper wire, 0.5 mm in diameter, with a 5 mm ferrite core diameter. The inductance rating ranges from 10 μ H to 1000 μ H and this specification is suitable for the proposed MIT system, which only requires approximately 35 μ H. Figure 2 shows a dimensional drawing of the excitation coil provided by EPCOS. The square-type electromagnetic screen is made from 1 mm thick aluminium, cut to specific dimensions and shaped by hand. The dimensions of the screen, shown in Figure 3, are: outer dimensions of 42 \times 42 \times 22 mm and 21 mm intruding depth. An electromagnetic screen covers every excitation and receiving coil; 16 pieces were fabricated in total.



Figure 1 - Excitation coil mounted to a square-type electromagnetic screen

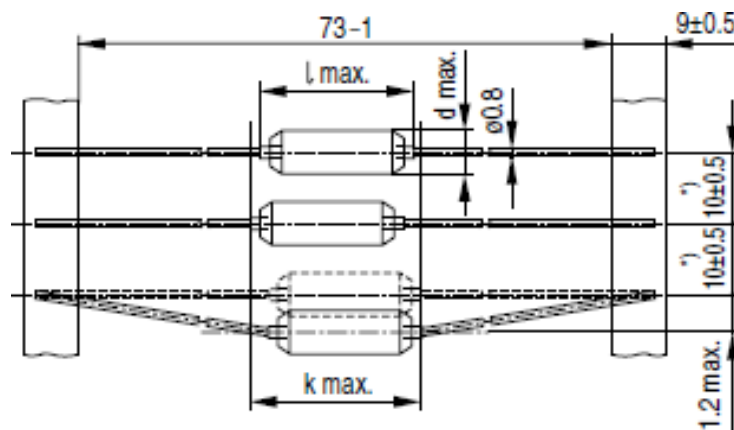


Figure 2 - Excitation coil dimensions [18]

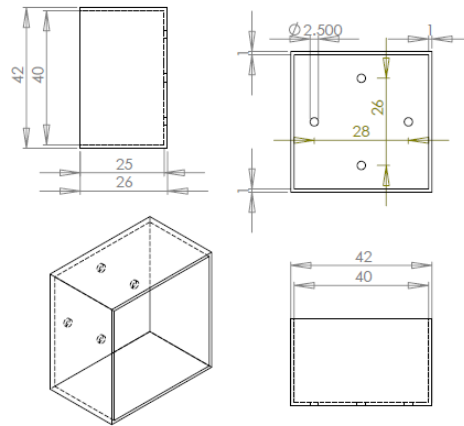


Fig. 3 - Square-type aluminium electromagnetic screen dimensions

The receiving coil, shown in Figure 4, is hand made using 0.5 mm diameter copper wire, wound into 200 turns on a ferrite core 2.5 mm in diameter. Similar to the excitation coil, the receiving coil is also mounted in a square type electromagnetic screen in order to minimise the effect of noise from the adjacent coils. The magnetic field produced by the excitation coil of this architecture is frequency dependent, therefore the GFB-8255A function generator was used for signal generation.



Fig. 4 - Hand wound receiving coil with 200 turns

2.2 Sensor Fixture Design

Sensor socket fixture jigs were used to mount and fix all 16 sensing coils in the square-type electromagnetic screen to form a circular array. As was mentioned earlier, both excitation and receiving coils have been chosen and precisely fabricated so that they can be mounted and arranged in the 16 corresponding sockets. Figure 5 shows the socket fixture before placing the sensors, while Figure 6 shows the socket fixture complete with 16 sensing coils with square type electromagnetic screens. The manufactured sensor fixtures were designed using SolidWorks 2009.

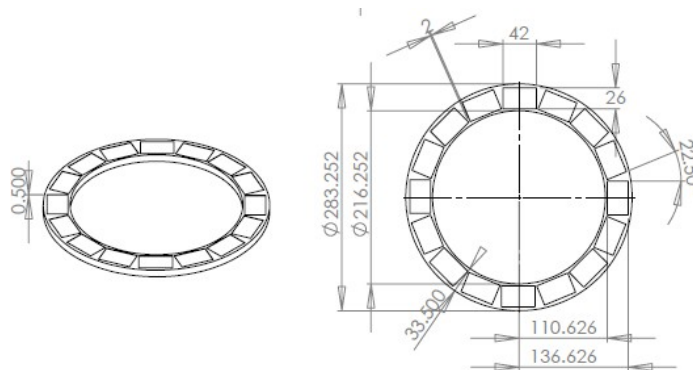


Fig. 5 - Sensor socket fixture for 16 sensing coils

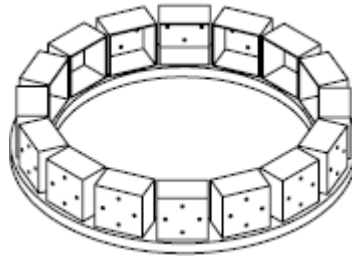


Fig. 6 - Sensor socket fixture with 16 square-type electromagnetic screens to contain the sensing coils

2.3 Sensor arrangement

Figure 7 shows the sensor arrangement within the jig. The excitation coils, coloured red, and the receiving coils, in blue, were arranged alternately within the fixture. The angle between an excitation coil and an adjacent receiving coil is 22.5° . The material used to fabricate the fixture was a synthetic fibre of poly acrylonitrile, more commonly known as acrylic plastic.

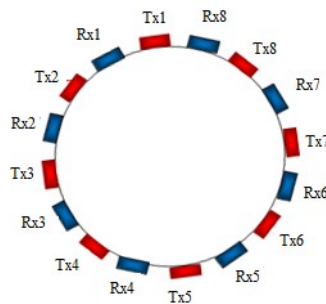


Fig. 7 - Arrangement of the excitation coils (Tx) and receiver coils (Rx) in the developed MIT system

2.4 Electronic measurement circuits

The electronic measurement circuit system can be divided into two individual subsystems:

- Transmitter circuit;
- Receiver and signal conditioning circuit.

2.4.1 Transmitter circuit

The transmitter circuit was designed using an operational amplifier that had the following features: low noise, high speed, high output current drive capability, fast settling time (>40 ns) and low cost. The op-amp used, AD817 from Analog Devices, fulfilled all stated requirements. These ICs have high unity gain bandwidth, 50 MHz, and a fast settling time of 45 ns enabling use for the amplification of a 500 kHz sine wave in the excitation circuit. Figure 8 shows the amplifier circuit with the AD817 op-amp.

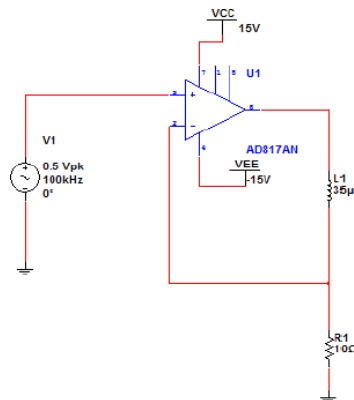


Fig. 8 - Signal amplifier circuit

In electronic circuitry, an amplifier is a circuit that can increase the amplitude of a signal by controlling the output signal with respect to the input signal. A non-inverting amplifier configuration was used because it offers higher input impedance than the inverting amplifier circuit. The gain of a non-inverting amplifier can be determined

using Equation 3.1:

$$Av = 1 + R_1/R_2 \tag{3.1}$$

When the non-inverting input (V+) is at a higher voltage than the inverting input (V-), the high gain of the op-amp causes it to output the greatest positive voltage it can. When the non-inverting input (V+) drops below the inverting input (V-), the op-amp outputs the greatest negative voltage it can. This relationship can be written in equation form as follows:

$$\begin{aligned} &\text{If } V^+ > V_{re}^- \text{ then } V_{out} = +V_{cc}, \\ &\text{If } V^+ < V_{re}^-, \text{ then } V_{out} = -V_{cc}. \end{aligned} \tag{3.2}$$

The magnetic field produced by the excitation coil in this architecture is frequency dependent, therefore the GFB-8255A function generator has been used to generate the signal. In the literature [6,16], some implementations of biomedical MIT use a crystal oscillator as a sine wave signal source that is fed to the excitation circuit, to avoid the influence of the primary field being captured by the receiver. This can be achieved because biomedical MIT measures the low conductivity of biological tissue, but is not suitable for imaging high conductivity materials such as copper and steel phantoms.

2.4.2 Receiver and signal conditioning circuit

The receiver section consists of a receiving coil, the signal conditioning circuit and a microcontroller. The signal detected at the receiver coil is simultaneously transferred to the signal conditioning circuit for processing. At this stage, the signal has to undergo five processing stages; pre-amplification, amplification, peak detection, isolation amplification and buffering as shown in Figure 9, before it is sent to the microcontroller and computer for image reconstruction.



Fig. 9 - Receiver and signal conditioning circuit block diagram

2.4.3 Preamplifier

The preamplifier is the first stage that the received signal from the receiver coil will reach. The received signal at the receiver coil is very low, in the mV range, thus the instrumentation amplifier INA111, shown in Figure 10, was selected. INA111 has the capability to amplify the mV range of the signal, and has high speed, high slew rate and low noise. This FET-input instrumentation amplifier also offers excellent performance due to its current-feedback topology, which provides an extended bandwidth (2 MHz at gain=10) and fast settling time (4 μs at gain=100). The range of the gain can be varied from 1 to more than 1000, and is set by a single external resistor. The input impedance of the INA111 is extremely high, approximately 10¹² Ω. However, a path must be provided for the input bias current of both inputs. The input bias current is typically less than 10 pA. High input impedance means that this input bias current changes very little with varying input voltage.

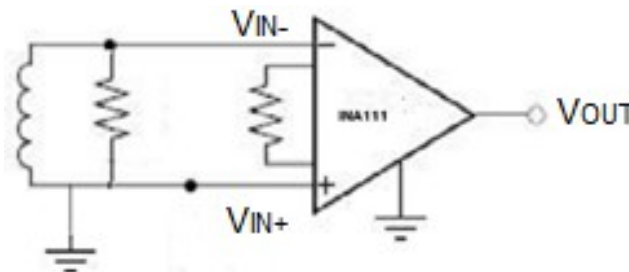


Fig. 10 - Preamplifier circuit using INA111 (gain can be varied from 1 to more than 1000)

2.4.4 Amplifier

The AD817 op-amp has been chosen for the amplifier circuit as it was also used in the transmitter circuit. The AD817 is a low cost, low power device which can operate on single or dual supply, and is a high speed op amp. The

non-inverting amplifier configuration was used, as shown in Figure 11. Choice of the AD817 op-amp as the amplifier was due to its high speed characteristics, with 50 MHz unity gain bandwidth, 350 V/ μ s slew rate and a settling time of 45 ns (0.1%). Furthermore, it has low noise characteristics.

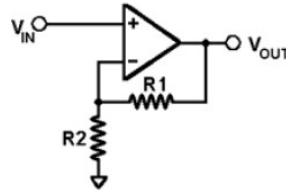


Fig. 11 - Amplifier using AD817

2.4.5 Peak detector

Due to its high speed characteristics, AD817 was also used to build a fast peak detector. The peak detector shown in Figure 12 was used to hold the maximum value of the input signal before the signal was measured, through application of a capacitor, to store the peak voltage value. When the input voltage increased, the capacitor was charged up to hold the new peak value, and if the input voltage decreased, the diode kept the capacitor from being discharged. The IN4148 diode was chosen for its high speed reverse recovery time, 4 ns. The second op-amp was used only as buffer.

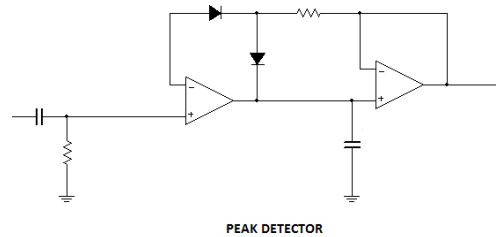


Fig. 12 - Peak detector in signal conditioning unit

2.4.6 Isolation amplifier

The isolation amplifier, shown in Figure 13, protects the data-acquisition components from the potentially destructive voltages present at remote transducers. These amplifiers are also useful when amplifying low-level signals in multi-channel applications. They can eliminate measurement errors caused by ground loops. The ISO124 was chosen for this project due to its low-cost precision isolation amplifier, which incorporates a novel duty cycle modulation- demodulation technique. In ISO124, the signal is transmitted digitally across a 2 pF differential capacitive barrier. The barrier characteristics do not affect signal integrity due to digital modulation, resulting in excellent reliability and good high-frequency transient immunity across the barrier. Both barrier capacitors are imbedded in the plastic body of the package. The nonlinearity of ISO124 is very low, 0.01%.

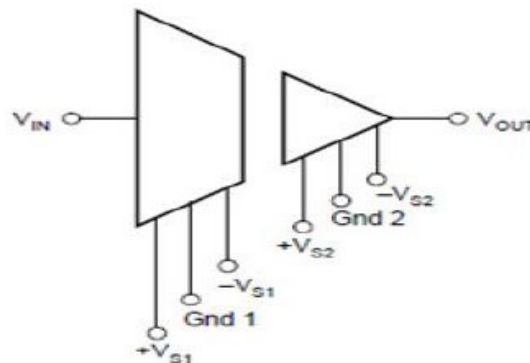


Fig. 13 - Internal structure of the isolation amplifier

2.4.7 Buffer

The buffer is used to avoid signal loss when connecting to a circuit with low input impedance. The HA5002 buffer was chosen for this project. HA5002, shown in Figure 14, has a high input impedance (300 k Ω) with low

output impedance (3 Ω). The HA5002 buffer can be used at high speed due to its very wide bandwidth (110 MHz) and very high slew rate (1300 V/μs).

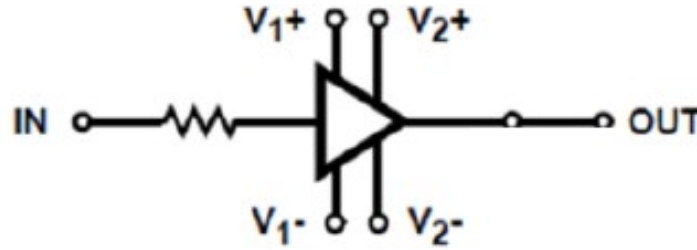


Fig. 14 - Internal structure of the HA5002 buffer

2.5 Voltage calculation

The voltage calculation was used to obtain the voltage sensed by the receiving coil. The value tabulated in the sensitivity map represents the digital value of ADC because the electronic measurement only reads the binary sequence.

$$V_{in} = \frac{D_{out} \times 5}{1023} \tag{3.3}$$

D_{out} is the digital value of ADC and V_{in} is the voltage input at the receiver.

2.6 Physical phantom

Four physical phantoms were used in the experiments to represent materials with certain conductivities. The phantoms used were two units of steel pipe and two units of copper pipe, as shown in Figure 15. The dimensions of the steel pipe are given in Table 3.1.

Table 3.1 - Dimensions and conductivity of four physical phantoms

Physical phantom	Thickness (mm)	Outer diameter (mm)	Conductivity, σ (S/m) at 20°C
Carbon steel pipe A	2.40	59.88	6.99×10^6
Carbon steel pipe B	2.40	34.00	6.99×10^6
Copper pipe A	1.28	22.00	5.96×10^7
Copper pipe B	1.28	17.58	5.96×10^7



Fig. 15 - (a) Steel pipe A, (b) steel pipe B, (c) copper pipe A and (d) copper pipe B

3. Results

The measurements were carried out on two experimental designs; single phantom imaging and dual phantom imaging. The measurement results are shown below.

3.1 Single phantom imaging

From the imaging tomogram below, the sensors are initially able to map the conductivity profile of the simple copper phantom model. The smearing effect can be clearly seen in (d), (e), (f), (g), (i), (j), (k) and (l).

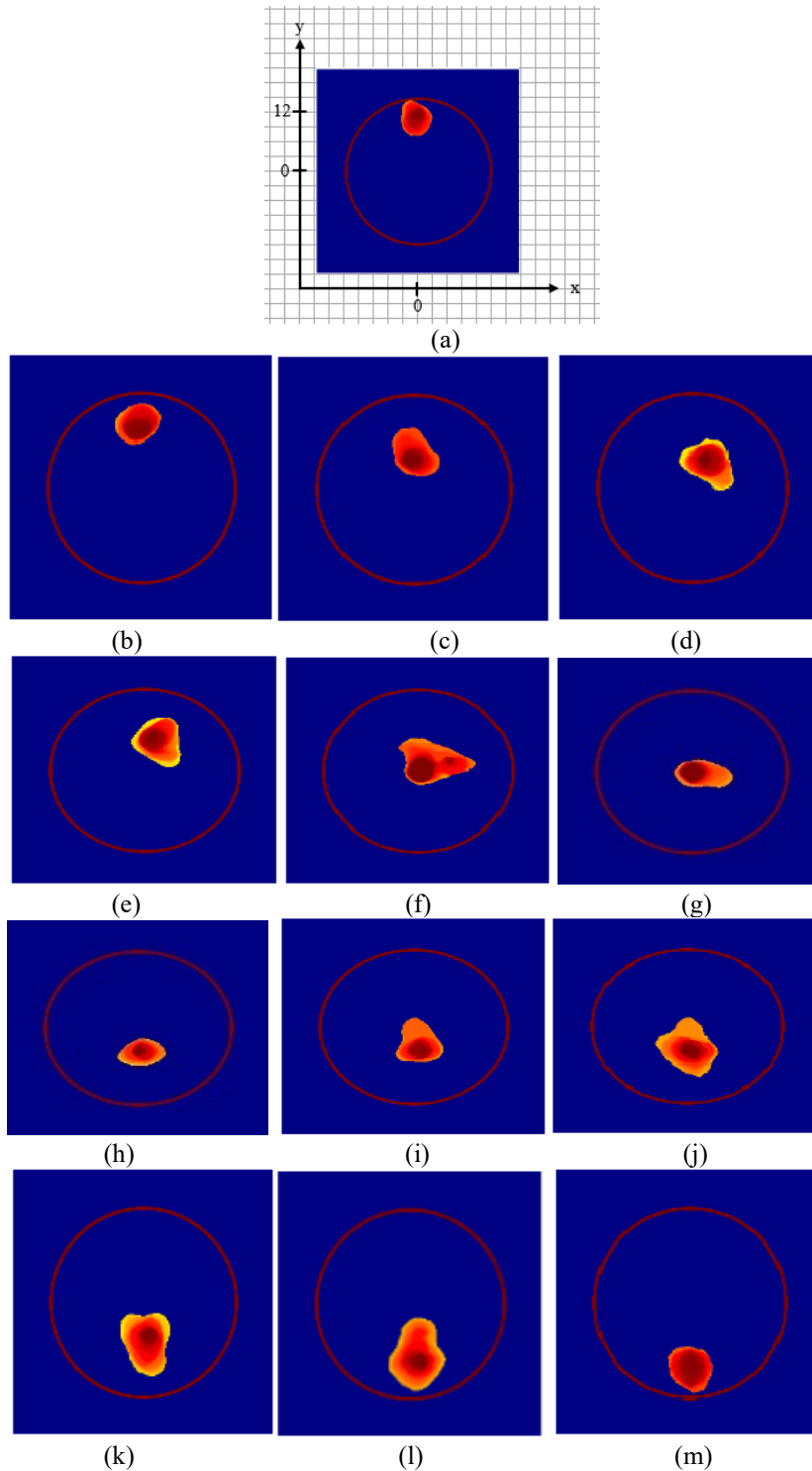


Fig. 16 - The tomograms for the single copper phantom model for changing y-axis position. (a) 12, (b) 10, (c) 8, (d) 6, (e) 4, (f) 2, (g) 0, (h) -2, (i) -4, (j) -6, (k) -8, (l) -10 and (m) -12

3.2 Dual phantom imaging

Copper 1 and copper 2 are pipes of 18 mm and 27 mm diameter, respectively, and have been positioned with respect to the y-axis. In all three cases, copper 1 has been moved towards the centre of the ROI while copper 2 stay in the same position. The smearing effect appears as copper 1 approaches copper 2, due to the non-linearity of the MIT

when using the linear reconstructed algorithm. The lack of colour gradient is due to fewer sensors having been used, and it is agreed that the resolution of the images can be enhanced by increasing the number of sensors.

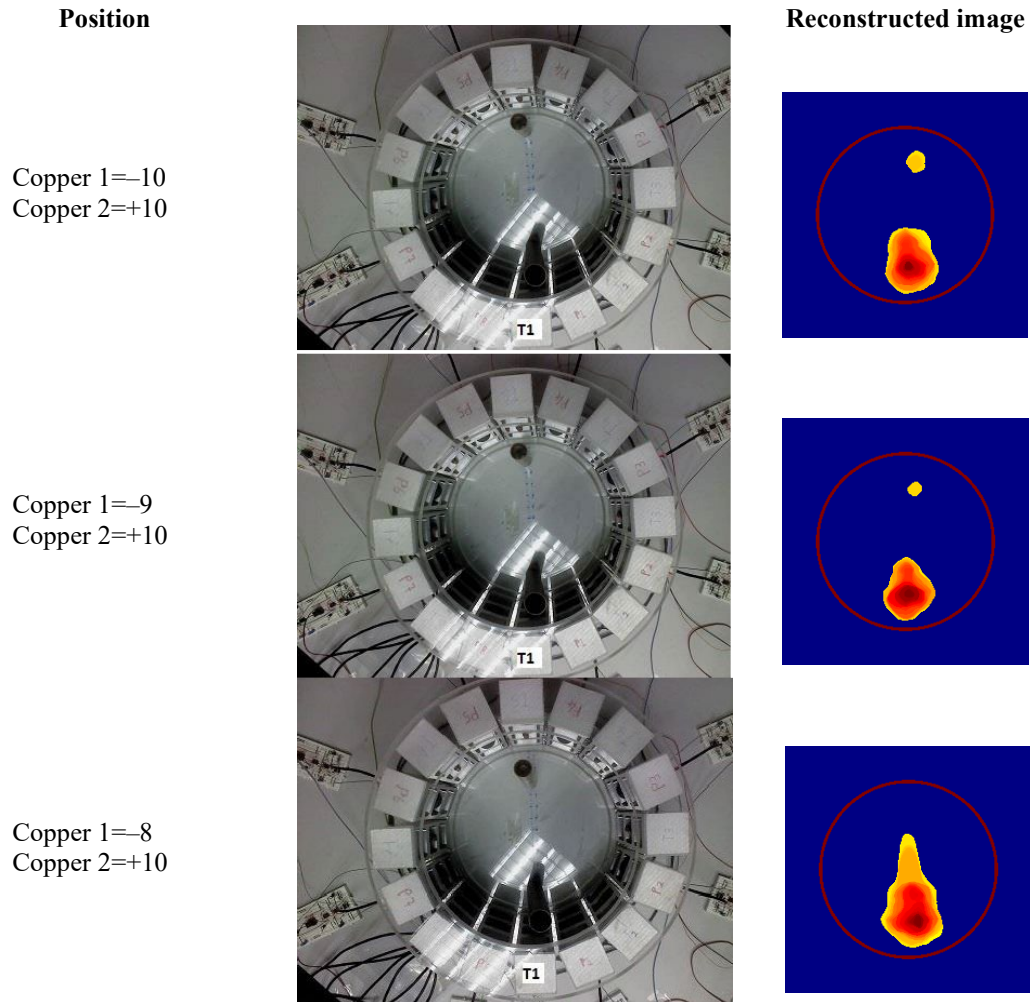


Fig. 16 - Dual phantom tomogram

4. Conclusions

A small scale non-invasive imaging system using MIT has been successfully developed. Evaluation of the system's imaging performance and analysis for four different physical phantoms has been presented. The small scale non- invasive and low cost sensing coil as a sensor operating at 500 kHz has been successfully designed for conductivity measuring purposes. This has been completed through several test stages on both single channel and full channel sensors. The hardware components were then successfully integrated with the software components through the synchronisation of both divisions. The linear back projection image reconstruction algorithm was found to be suitable and able to process the data to map the conductivity profile of the steel and copper pipe phantoms. The image reconstruction was carried out in an off-line method. The imaging results showing the conductivity profile of the respective phantoms were presented in section result.

Acknowledgement

The authors would like to acknowledge the Gleneagles Hospital Medini, Universiti Teknologi Malaysia, Universiti Malaysia Perlis and KAIFA Technology Malaysia Sdn. Bhd.

References

- [1] Wei, H.-Y. and Soleimani, M. (2012). A Magnetic Induction Tomography System for Prospective Industrial

- Processing Applications. Chinese Journal of Chemical Engineering. 20, 406-410
- [2] Xiandong, M., Peyton, A. J., Binns, R., Higson, S. R. (2005). Electromagnetic Techniques for Imaging The Cross- Section Distribution of Molten Steel Flow In The Continuous Casting Nozzle. Sensors Journal. IEEE, 5, 224-232
- [3] Ida, N. & Lord, W. (1983). 3-D Finite Element Predictions of Magnetostatic Leakage Fields. Magnetics, IEEE Transactions on. 19, 2260-2265
- [4] Williams, R. A. and Beck, M. S. (1995). Process Tomography: Principles, Techniques, and Applications, Butterworth-Heinemann
- [5] Goss, D., Mackin, R., Crescenzo, E., Tapp, H. S. And Peyton, A. J. (2003). Development of Electromagnetic Inductance Tomography (EMT) Hardware for Determining Human Body Composition. Proc. 3rd World Congress on Industrial Process Tomography
- [6] Peyton, A., Mackin, R., Goss, D., Wan-Daud, W., Crescenzo, E., Saunders, N. and Tapp, H. (2003). Addressing the Difficulties in Using Inductive Methods to Evaluating Human Body Composition. Biométrie Humaine et Anthropologie, 21, 63-71
- [7] Moissl, U. M., Wabel, P., Chamney, P. W., Bosaeus, I., Levin, N. W., Bost Westphal, A., Korth, O., Müller, M. J., Ellegard, L., Malmros, V., Kaitwatcharachai, C., Kuhlmann, M. K., Zhu, F. and Fuller, N. J. (2006). Body Fluid Volume Determination via Body Composition Spectroscopy in Health and Disease. Physiol Meas, 27(9), 921-33
- [8] Higgins, K. J., Reid, P. M., Going, S. B. and Howell, W. H. (2007). Validation of Bioimpedance Spectroscopy to Assess Acute Changes in Hydration Status. Med Sci Sports Exerc, 39(6), 984-90
- [9] Zou, Y. and Guo, Z. (2003). A Review of Electrical Impedance Techniques for Breast Cancer Detection. Medical Engineering & Physics. 25(2), 79-90
- [10] Hartov, A., Soni, N. and Halter, R. (2004). Breast Cancer Screening With Electrical Impedance Spectroscopy, in Holmer, N. G., ed. Electrical Impedance Tomography: Methods, History and Applications, Institute of Physics
- [11] Halter, R. J., Hartov, A., Heaney, J. A., Paulsen, K. D. and Schved, A. R. (2007). Electrical impedance spectroscopy of the human prostate. IEEE Trans Biomed Eng, 54(7), 1321-7
- [12] Merwa, R., Hollaus, K., Oszkar, B. and Scharfetter, H. (2004). Detection of Brain Oedema Using Magnetic Induction Tomography: A Feasibility Study of the Likely Sensitivity and Detectability. Physiological Measurement, 25(1), 347- 354
- [13] Zolgharni, M., Ledger, P. D., Griffiths, H. (2009). Forward Modelling of Magnetic Induction Tomography: A Sensitivity Study for Detecting Haemorrhagic Cerebral Stroke. Medical & Biological Engineering & Computing. 47. 1301- 1313
- [14] Sin, K., Van. and Anderson, C., R. (1998). Method and Apparatus for Measurement of Whole Blood Coagulation Parameters. WO/1998/039643
- [15] Spence, N. (2002). Electrical Impedance Measurement as an Endpoint Detection Method for Routine Coagulation Tests. Br J Biomed Sci. 59(4), 223-7
- [16] Hartov, A., Soni, N. and Halter, R. (2004). Breast Cancer Screening With Electrical Impedance Spectroscopy, in Holmer, N. G., ed. Electrical Impedance Tomography: Methods, History and Applications, Institute of Physics
- [17] Bauman, J. H. and Hoffman, R. W. (1967). Magnetic Susceptibility Meter for In Vivo Estimation of Hepatic Iron Stores. IEEE Trans Biomed Eng, 14(4), 239-43
- [18] Tumanski, S. (2007). Induction Coil Sensors—A Review. Measurement Science and Technology, 18, R31